Targeting the STAT5A/IDO1 axis overcomes radioresistance and reverses the immunosuppressive tumor microenvironment in NSCLC

YANG YANG[1], XIAOLI ZHENG[1], PEIZAN NI[1], DINGJIE LI[1], QINFU DAN[1], XIAOHUI WANG[1], YUNHAN WANG[1], YANAN SUN[1], KANGDONG LIU[2,3], ZIGANG DONG[2,3] and HONG GE[1]

[1]Department of Radiation Oncology, The Affiliated Cancer Hospital of Zhengzhou University and Henan Cancer Hospital; [2]Department of Pathophysiology, China-US (Henan) Hormel Cancer Institute, Zhengzhou, Henan 450008; [3]Department of Pathophysiology, The School of Basic Medical Sciences, Zhengzhou University, Zhengzhou, Henan 450001, P.R. China

Received April 7, 2022; Accepted October 24, 2022

DOI: 10.3892/ijo.2022.5460

Abstract. As a metabolic mediator of antitumor immunity, indoleamine-2,3-dioxygenase 1 (IDO1) is upregulated in various types of cancer; however, the regulatory mechanism and clinical significance of IDO1 in non-small cell lung cancer (NSCLC) radiotherapy (RT) remain unclear. The present study investigated the role of IDO1 in the NSCLC microenvironment. MTT assay, immunofluorescence, apoptosis analysis, cell cycle analysis, and C57BL/6 and BALB/c nude mouse tumor models were utilized to evaluate the roles of the STAT5A/IDO1/kynurenine axis in radioresistance and in the immune microenvironment of NSCLC. Protein expression levels were evaluated by western blotting, immunofluorescence and immunohistochemistry. Flow cytometry was performed to assess the status of $CD8^+$ T lymphocytes, regulatory T cells (Tregs) and immune-related inflammatory factors in C57BL/6 mice. Notably, IDO1 and STAT5A were positively associated with the immune microenvironment. RT treatment significantly promoted the expression levels of IDO1. IDO1 knockdown markedly enhanced the radiosensitivity of lung tumor cells and the anti-apoptotic properties of T lymphocytes. It was demonstrated that STAT5A knockdown suppressed T-cell apoptosis by inhibiting IDO1 enzyme function. Finally, *in vivo* experiments showed that STAT5A knockdown combined with RT was associated with greater numbers of $CD8^+$ T cells and fewer Tregs. Results from the present study indicated that targeting the STAT5A/IDO1 axis may reshape the immune microenvironment and promote the efficacy of RT in NSCLC treatment. The present study may provide a theoretical foundation for more efficient use of immunotherapy regimens in NSCLC treatment.

Correspondence to: Professor Hong Ge, Department of Radiation Oncology, The Affiliated Cancer Hospital of Zhengzhou University and Henan Cancer Hospital, 127 Dong Ming Road, Zhengzhou, Henan 450008, P.R. China
E-mail: gehong616@126.com

Professor Zigang Dong, Department of Pathophysiology, The School of Basic Medical Sciences, Zhengzhou University, 100 Kexue Avenue, Zhengzhou, Henan 450001, P.R. China
E-mail: dongzg@zzu.edu.cn

Abbreviations: FOXP3, forkhead box P3; IDO1, indoleamine-2,3-dioxygenase 1; IHC, immunohistochemistry; KYN, kynurenine; NSCLC, non-small cell lung cancer; RT, radiotherapy; SBRT, stereotactic radiotherapy; TME, tumor microenvironment; TRP, tryptophan

Key words: NSCLC, STAT5A, IDO1, radioresistance, immune escape

Introduction

Lung cancer is one of the main health burdens worldwide; non-small cell lung cancer (NSCLC) accounts for ~85% of lung cancer cases, with most patients diagnosed at a metastatic or advanced stage (1,2). For patients with locally advanced NSCLC, concurrent chemoradiotherapy is the backbone of treatment; however, the efficacy of chemotherapy is hampered by the emergence of NSCLC recurrence and distant metastasis (3,4). Radiotherapy (RT), particularly stereotactic body RT (SBRT), exerts beneficial effects on the tumor microenvironment (TME) (5-7). For example, lethal dose irradiation can induce immunogenic cell death; non-lethal dose irradiation can alter the immunological phenotype of tumor cells (such as by upregulating the expression of tumor MHC-I molecules) and can enhance the ability of T cells to kill tumor cells. However, RT can also recruit immunosuppressive cells to aggregate in tumor tissues, induce immune checkpoint generation [e.g., programmed cell death 1 ligand 1 (PD-L1)] and promote tumor immune tolerance (8-10). Our previous study reported that increasing the dose of SBRT cannot improve its curative effect (11). Moreover, the 4-year failure rate of SBRT in the treatment of early NSCLC was 38% (12). Treatment with SBRT alone is not enough to change the immunosuppressive TME. It is still difficult to trigger a systemic antitumor immune effect

even though RT can result in the release of tumor antigens locally in the lesion (7).

In recent years, the use of immune checkpoint inhibitors, including programmed cell death protein 1 (PD-1) and PD-L1, has transformed tumor therapy, promoting significant clinical outcomes in numerous tumor types (13-15). In addition, it has been reported that the TME contains inhibitory factors, including CTLA-4, TIM-3, LAG-3, CD160 and indoleamine 2,3-dioxygenase 1 (IDO1) (16). IDO1 is a rate-limiting enzyme that catalyzes the conversion of tryptophan (TRP) to kynurenine (KYN) for immune regulation. IDO1 is upregulated in some types of cancer (such as colorectal, esophageal and breast cancer) and can lead to immune escape and metastasis, resulting in poor patient prognosis (17-19). The high expression levels of IDO1 leads to TRP depletion and the accumulation of metabolites (such as KYN, kynurenic acid and 3-hydroxykynurenine), to activate general control nonderepressible 2 (GCN2). The activation of GCN2 can block the cell cycle of T cells or induce apoptosis, thereby mediating the immune escape of tumor cells (20). Emerging studies, including our previous study, have reported that a high expression of IDO1 is positively associated with poor cancer prognosis (21,22). Furthermore, IDO1 may regulate the sensitivity of tumor cells to RT and chemotherapy drugs (23,24), and could be associated with immunotherapeutic drug resistance (25,26). Although the major findings of IDO1 have been described, the association of IDO1 with RT in NSCLC remains ambiguous.

STAT5 has two subtypes, STAT5A and STAT5B, that are encoded by two genes in series on the human chromosome 17q21.2 (27). STAT5A is strongly associated with the occurrence and progression of various types of cancer, such as prostate cancer, breast cancer, malignant melanoma and lung cancer (28-30); it can inhibit cell apoptosis, promote tumor cell proliferation and invasion, and has been reported to be related to DNA repair in patients with chronic myeloid leukemia (31). Maranto *et al* (31) demonstrated that inhibiting STAT5 activation could increase the radiosensitivity of prostate cancer and reduce the ability of DNA repair. However, to the best of our knowledge, targeting STAT5A and IDO1 in lung cancer treatment has not been reported, and the effect of STAT5A on T-cell response through IDO1 in the lung cancer TME is not well characterized.

Therefore, the present study aimed to investigate the role of the STAT5A/IDO1 axis in RT-mediated immunosuppression in the NSCLC and to provide insights into the development of more efficient immunotherapy regimens for NSCLC treatment.

Materials and methods

Datasets and databases. The TIMER database (TIMER2.0, cistrome.shinyapps.io/timer; Immune Association dataset) is a web resource used for comprehensive analysis of tumor-infiltrating immune cells, which was established by the Department of Statistics, Harvard University and Dana-Farber Cancer Institute. The UCSC database (http://genome.ucsc.edu/cgi-bin/hgNear), the PROMO database (http://alggen.lsi.upc.es/cgi-bin/promo_v3/promo/promoinit.cgi?dirDB=TF_8.3) and GeneCards (https://www.genecards.org) are searchable, integrative database that provides comprehensive, user-friendly information on all annotated and can predict the transcription factor of genes.

Cell culture. The normal human bronchial epithelial cell line BEAS-2B, the human lung adenocarcinoma cell lines (A549, NCI-H1975, NCI-H1650, NCI-H460 and PC-9), the Jurkat T cells and the mouse Lewis lung carcinoma (LLC) cell line were purchased from The Cell Bank of Type Culture Collection of Chinese Academy of Sciences (https://cellbank.org.cn) and were stored at the Cancer Institute of Henan Cancer Hospital (Zhengzhou, China). The human lung adenocarcinoma cells, Jurkat T cells and BEAS-2B cells were cultured in conventional RPMI-1640 medium containing 10% FBS (Gibco; Thermo Fisher Scientific, Inc.), 100 U/ml penicillin and 100 mg/ml streptomycin, whereas the LLC cells were cultured in DMEM containing 10% FBS (Gibco; Thermo Fisher Scientific, Inc.), 100 U/ml penicillin and 100 mg/ml streptomycin.

Irradiation. Tumor cells (A549 and H1975) were seeded in 6-cm dishes and exposed to 0, 2, 4, 6, 8 or 10 Gy irradiation using an X-ray irradiator (Varian Medical Systems, Inc.). The irradiation field, source skin distance (that is, the distance from the center of radiation source to the center of body surface radiation field) and dose rate were 13x13 cm, 100 cm and 400 cGy/min, respectively. In addition, BALB/c nu/nu and C57BL/6 mice were exposed to 8 Gy irradiation after the tumor volume reached 100 mm^3 using a small animal radiation platform.

Cell transfection. The short hairpin (sh)IDO1-1 (5'-CCATCTGCAAATCGTGACTAA-3'), shIDO1-2 (5'-CGTAAGGTCTTGCCAAGAAAT-3'), shSTAT5A-1 (5'-GCGCTTTAGTGACTCAGAAAT-3'), shSTAT5A-2 (5'-GAGAAGTTCACAGTCCTGTTT-3') and scrambled control (Scr; 5'-TTCTCCGAACGTGTCACGT-3') sequences inserted into the GV248 lentiviral vector were purchased from Shanghai GeneChem Co., Ltd. (cat. no. CON077). A549 and H1975 cells were infected with the viral particles in 4% polybrene (cat. no. REVG005; Shanghai GeneChem Co., Ltd.) at a multiplicity of infection of 20. After 72 h of infection, the cells were cultured in complete medium containing 2 μl/ml puromycin to screen stable cell lines for 48 h. The GFP tag was carried in the shRNA lentiviral vector and used to observe the infection efficiency of lentivirus under fluorescent microscope.

RNA extraction and reverse transcription-quantitative PCR (qPCR). Total RNA was extracted from cells in the different treatment groups using TRIzol® (Invitrogen; Thermo Fisher Scientific, Inc.) and then reverse-transcribed to cDNA using a Reverse Transcription Kit (cat. no. RR047A; Takara Bio, Inc.). The cDNA was then used as the template for qPCR using a SYBR Premix Ex Taq kit (Takara Bio, Inc.) on an Applied Biosystems Real-time PCR System (Thermo Fisher Scientific, Inc.). The thermocycling conditions were as follows: 95˚C for 30 sec; followed by 40 cycles of denaturation at 95˚C for 5 sec and annealing at 60˚C for 30 sec. GAPDH was used as an internal control. Relative RNA expression levels were calculated by the $2^{-\Delta\Delta Cq}$ method (33). The primer sequences were as follows: IDO1 forward, 5'-GCCTGATCTCATAGAGTCTGGC-3' and reverse, 5'-TGCATCCCAGAACTAGACGTGC-3';

GAPDH forward, 5'-GTCTCCTCTGACTTCAACAGCG-3' and reverse, 5'-ACCACCCTGTTGCTGTAGCCAA-3'.

Western blot analysis. Cells were lysed with RIPA lysis buffer (Beyotime Institute of Biotechnology) on ice for 30 min, centrifuged at 20,000 x g for 30 min at 4˚C and the supernatant was collected to obtain total proteins. The protein concentration was determined by the BCA assay (Thermo Fisher Scientific, Inc.) according to the manufacturer's protocol. Equal amounts (40 μg) of cell lysates were separated by 8-12% SDS-PAGE and transferred to a polyvinylidene difluoride membrane (Bio-Rad Laboratories, Inc.). The membrane was subsequently blocked for 1-2 h using 5% non-fat milk at room temperature, then incubated with the primary antibodies (1:1,000 dilution) at 4˚C overnight. After washing with TBS + 0.05% Tween 20, the membrane was incubated with the secondary antibody for 2 h at room temperature. Proteins were visualized using the SuperSignal™ West Pico PLUS Chemiluminescent Substrate (cat. no. 34580; Thermo Fisher Scientific, Inc.), and a gel electrophoresis image analyzer (LI-COR Biosciences) was used for color development. The primary and secondary antibody details are shown in Table SI.

Cell immunofluorescence assay. Sterile glass coverslips were placed in 24-well plates, and $2x10^4$ cells were seeded into the wells. The cells were exposed to 8 Gy RT for 6, 12, 24 or 48 h. After washing with PBS, the cells were fixed with 4% paraformaldehyde for 15 min at room temperature, incubated with 5% bovine serum albumin (cat. no. ST023-1000g; Beyotime Institute of Biotechnology) at room temperature for 30 min. Subsequently, a primary antibody (anti-IDO1; 1:100; cat. no. 13268-1-AP; Proteintech Group, Inc.) was added to the cells at 4˚C for 15 h and the cells were then incubated with Alexa Fluor 488 goat anti-rabbit IgG (1:400; cat. no. A11008; Invitrogen; Thermo Fisher Scientific, Inc.) at room temperature for 2 h. Finally, the coverslips were mounted onto glass slides with anti-fluorescence quenching sealing agent containing DAPI (ProLong™ Gold Antifade Mountant; cat. no. P36930; Invitrogen; Thermo Fisher Scientific, Inc.) and imaged using a Leica SP5II confocal microscope (Leica Microsystems GmbH).

Cell co-culture system. Jurkat T cells were used as a model for the analysis of the anti-T cell proliferation effect of the cancer cell culture supernatant, as previously described (34). H1975 cells ($1x10^5$) in 800 μl RPMI-1640 with 10% FBS were added to the bottom of the Transwell chamber. The Jurkat T cells ($2x10^5$) in 300 μl RPMI-1640 with 10% FBS were added to the upper chamber. The cells were co-cultured at 37˚C for 24 h. Finally, western blot analysis and flow cytometry were used to detect apoptosis of Jurkat T cells. The following four groups were established: i) Negative control group; ii) EPA group; iii) RT group; iv) EPA + RT group. H1975 cells were pretreated for 1 h at 37 with 10 μmol/l EPA (Selleck Chemicals; dissolved in DMSO), a selective IDO1 inhibitor, and then treated with RT as aforementioned. The following six groups were also established: i) Scr group; ii) shIDO1#1 group; iii) shIDO1#2 group; iv) RT-only group; v) shIDO1#1 + RT group; vi) shIDO1#2 + RT group. An additional set of experiments included the following groups: i) Scr group; ii) shSTAT5A#1 group; iii) shSTAT5A#2 group; iv) RT-only group; v) shSTAT5A#1 + RT group; vi) shSTAT5A#2 + RT group.

Colony formation assays. Transduced A549 and H1975 cells (Scr, shIDO1#1, shIDO1#2; shSTAT5A#1, shSTAT5A#2) were seeded (1,000 cells/well) in 6-well plates in 2 ml medium and incubated for 24 h. Subsequently, cells were exposed to 0, 2, 4, 6 or 8 Gy irradiation using an X-ray irradiator and were further incubated for an additional 14 days. The medium was then removed and cells were fixed with 0.1% formaldehyde at room temperature for 20 min; 0.5% crystal violet was used to stain the colonies for 10 min at room temperature. The dye solution was slowly rinsed away with distilled water and the cells were air-dried. A colony was considered as having >50 cells, and visualized under an IX73 inverted optical microscope (Olympus Corporation) and the number of colonies was counted using ImageJ software (version 1.51K; National Institutes of Health). The classic multitarget single-hit model was applied to plot the dose survival curves. Survival fraction (SF)=1-(1-$e^{-D/D0}$) N, where the mean lethal dose (D0) represents the dose needed to decrease the fraction of surviving cells to 37% of its previous value, N is the extrapolation number, and the quasi-threshold dose (Dq) indicates repair capacity of tumor cells after radiation therapy. Radiation sensitivity parameters included survival fraction at 2 Gy (SF2), D0, Dq and the sensitivity enhancement ratio was calculated. The sensitivity enhancement ratio was calculated by dividing D0 in the control group by D0 in the treatment group. The test was repeated three times.

Cell cycle analysis by flow cytometry. Cells were seeded in 6-well plates at a density of $1x10^6$ cells/well, then divided into the six experimental groups (Scr, shSTAT5A#1, shSTAT5A#2, RT, shSTAT5A#1 + RT and shSTAT5A#2 + RT). After 24 h of treatment, the cells were harvested, washed with phosphate-buffered saline (PBS) and fixed with 70% ice-cold ethanol at -20˚C overnight. The cells were then washed further with PBS and stained using the CycletestPlus DNA Reagent kit (BD Biosciences, San Jose, CA, USA), according to the manufacturer's protocol. The cell cycle distribution was analyzed by a flow cytometer (BD Biosciences).

Apoptosis analysis by flow cytometry. For apoptosis, transfected A549 and H1975 cells were seeded into 6-well plates. Once they reached confluence (60-70%), the cells were collected and incubated with Annexin V-FITC (5 μl; Biogot Technology Co., Ltd.) and propidium iodide solution (5 μl; Biogot Technology Co., Ltd.) at room temperature for 15 min according to the manufacturer's instructions. Cells were subsequently suspended in 400 μl binding buffer (Biogot Technology Co., Ltd.). Early + late stage apoptosis was analyzed using a FACSAria flow cytometer (BD Biosciences). All data were analyzed with ModFit version 4.0 (Verity Software House, Inc.).

ELISA. The A549 and H1975 cell culture supernatants were directly collected, and then the concentration of KYN was determined with a Human KYN ELISA kit (CUSABIO; catalog number CSB-E13659h) according to the manufacturer's instructions.

Animal studies. Mice were purchased from Beijing Vital River Laboratory Animal Technology Co., Ltd. and were housed under pathogen-free conditions. All animal experiments were performed in accordance with the institutional guidelines and were approved by the Committee on the Ethics of Animal Experiments of Zhengzhou University (NO.CUHCI2021-003). The animals were housed under controlled environmental conditions: 12-h dark/light cycle; 20-22˚C; humidity, 55±5%, and were allowed free access to normal food and water. Two murine models were used in the present study and were established as follows: i) BALB/c nu/nu mice (age, 4-6 weeks; female; weight, 15-17 g) were subcutaneously injected with $5x10^6$ H1975 cells on their dorsal flanks; ii) C57BL/6 mice (age, 4-6 weeks; female; weight, 15-17 g) were subcutaneously injected with $5x10^6$ LLC cells, which are syngeneic to C57BL/6, on their dorsal flanks. The mice were randomly divided into four groups (n=6 for BALB/c nu/nu mice and n=5 for C57BL/6 mice): i) Scr group, ii) shSTAT5A group, iii) RT group and iv) shSTAT5A + RT group. Mice were subcutaneously inoculated in the right flank with $5x10^6$ NCI-H1975 and LLC cells with or without stable shSTAT5A transduction. The tumor sizes were recorded every 3 days for BALB/c nu/nu mice and twice per week for C57BL/6 mice. Tumor volume was measured with a digital caliper [(length x width^2)/2] and body weight was recorded periodically. The mice were sacrificed by intraperitoneal injection of sodium pentobarbital 20 days later (200 mg/kg) and death was verified by respiratory and cardiac arrest, and pupil dilation. Tumor ulceration, tissue swelling and cachexia were the humane endpoints evaluated, and none of the mice used in the study met these endpoints.

Flow cytometric profiling of lymphocytes. Mouse spleens were excised and ground through a 70-μm nylon mesh. Single spleen cells were then resuspended in PBS and lysed by Red Blood Cell Lysis Buffer (cat. no. C3702; Beyotime Institute of Biotechnology). Cells were Fc-blocked with TruStain FcX™ (anti-mouse CD16/3; Clone 93; BioLegend, Inc.) for 30 min at 4˚C. In addition, mouse tumor tissues were minced, underwent enzymatic digestion with 0.1% collagenase (cat. no. C5138; MilliporeSigma), hyaluronidase (0.1 mg/ml; cat. no. H6254; MilliporeSigma) and DNase IV (20 U/ml; cat. no. D5025; MilliporeSigma) in Hank's balanced salt solution (Gibco; Thermo Fisher Scientific, Inc.) and ground through a 70-μm nylon mesh. The filtrate was collected and lysed with the Red Blood Cell Lysis Buffer. A single cell suspension of $1-2x10^6$ tumor-infiltrating lymphocytes and spleen cells was used for cell surface and intracellular marker staining. The single cell suspension was incubated with a conjugated monoclonal antibody (BioLegend, Inc., unless otherwise stated) at 4˚C for 30 min. All antibodies used for flow cytometric analysis of mouse tumor samples and spleen are shown in Table SII. All samples were assessed using a Cytek Aurora flow cytometer (Cytek Biosciences) and analyzed using FlowJo software (FlowJo V10.5.3; Becton Dickinson).

Immunohistochemistry (IHC). IHC was performed on 10% formalin-fixed (at room temperature for 4 h) paraffin-embedded tumor tissue sections (4 μm). The paraffin-embedded sections were deparaffinized, underwent antigen retrieval using microwave heating in 10 mM citrate buffer (pH 7.0) at 80˚C for 20 min; endogenous peroxidases were blocked with 3% H_2O_2 (OriGene Technologies, Inc.) at room temperature for 30 min and the sections were blocked with 5% goat serum (Beyotime Institute of Biotechnology) for 40 min at room temperature before being incubated with the primary antibodies at 4˚C overnight. The tissue sections were incubated with primary antibodies at 4˚C overnight. The following primary antibodies were used for IHC: Rabbit anti-mouse IDO1 (1:1,000; cat. no. 122402; BioLegend, Inc.); rabbit anti-mouse CD8 (1:200; cat. no. bs-0648R; Bioss antibodies, Inc.), rabbit anti-STAT5A (1:200; cat. no. ab32043; Abcam, Inc.), rabbit anti-Ki67 (1:400; cat. no. ab15580; Abcam); and rabbit anti-human FOXP3 (1:100; cat. no. ab215206; Abcam, Inc.). Following incubation with the primary antibodies, the samples were incubated with HRP-conjugated goat anti-rabbit IgG secondary antibody (1:2,000 dilution; cat. no. 7074S; Cell Signaling Technology, Inc.) at room temperature for 1 h. The samples were stained using DAB (OriGene Technologies, Inc.) at room temperature for 5 min and counterstained with hematoxylin at room temperature for 1 min. The images were obtained using an IX73 inverted light microscope (Olympus Corporation). Integrated optical density of the IHC image data were quantitatively analyzed using Image-Pro Plus v.6.0 (Media Cybernetics, Inc.) image analysis software.

Statistical analysis. All quantitative data are presented as the mean ± standard deviation, and were analyzed using GraphPad Prism version 8.0 (GraphPad Software, Inc.) and SPSS 22.0 software (IBM Corp.). The unpaired Student's t-test and one-way ANOVA followed by Tukey's post hoc test were used for single-group comparisons and multiple comparisons, respectively. $P<0.05$ was considered to indicate a statistically significant difference. All analyses represented at least three independent *in vitro* experiments.

Results

Inhibition of IDO1 enhances the efficacy of radiation in vitro. To elucidate the functional role of IDO1 in NSCLC, the protein expression levels of IDO1 were detected in immortalized normal lung epithelial cells (BEAS-2B) and lung cancer cells. IDO1 expression was high in PC-9, A549 and H1975 cells, but not in H1650, H460 and BEAS-2B cells (Fig. 1A). Moreover, whether radiation affected the expression of IDO1 was explored. Lung adenocarcinoma cell lines (A549 and H1975) were irradiated with a gradient dose of radiation, and the expression of IDO1 was evaluated 48 h later. The results revealed that with the increase in irradiation dose, the protein expression levels of IDO1 were increased; with the highest expression detected in the 8 Gy (A549) and 6 Gy (H1975) (Fig. 1B). It has been reported that changes in KYN concentration evaluated using ELISA can reflect the effect of RT on IDO1 enzyme activity (35). The present study results demonstrated that KYN levels in the culture supernatant were initially increased in response to irradiation, peaking at 8 Gy (A549) and 6 Gy (H1975), and then decreased (Fig. 1C). To further examine the effect of radiation on IDO1 expression, immunofluorescence was used to detect the localization of IDO1 in irradiated lung adenocarcinoma cells (Fig. S1). IDO1 expression was detected 12 h after irradiation and peaked

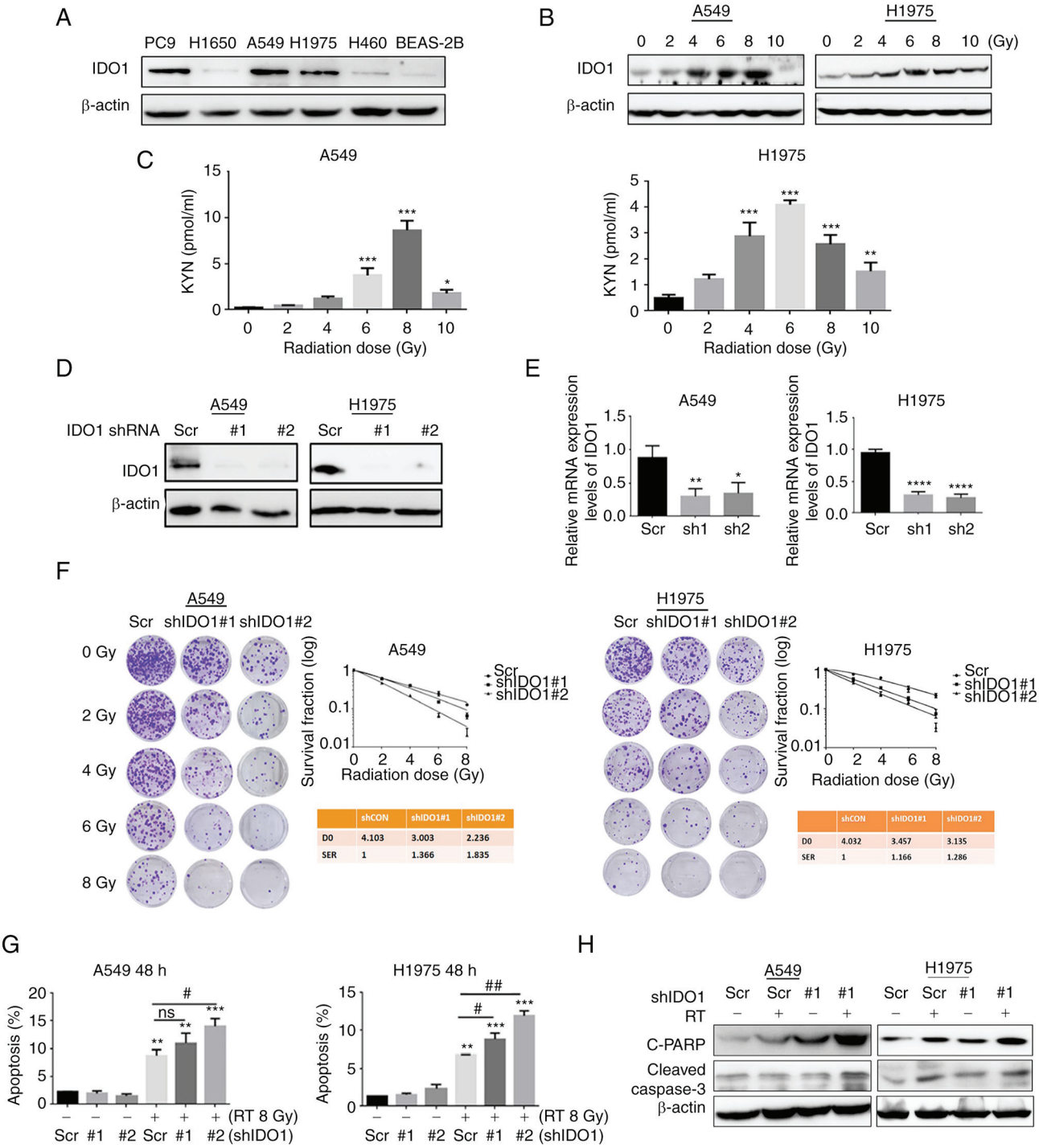

Figure 1. Radiation increases IDO1 expression in NSCLC cells and knockdown of IDO1 enhances radiosensitivity *in vitro*. (A) IDO1 protein expression levels in the human normal bronchial epithelial cell line BEAS-2B and NSCLC cell lines. (B) Protein expression levels of IDO1 in lung adenocarcinoma cells 48 h after gradient radiotherapy (lower panel). (C) ELISA was performed to detect KYN levels in A549 and H1975 cell supernatants 48 h after irradiation. IDO1 knockdown in A549 and H1975 cells, as determined by (D) western blotting and (E) reverse transcription-quantitative PCR. (F) Tumor cells were transduced with lentiviruses carrying Scr, shIDO1#1 or shIDO1#2) and were selected with 2 μg/ml puromycin. The surviving cells were then used to examine radiosensitivity following γ-irradiation (0, 2, 4, 6 or 8 Gy) by clonogenic assay. (G) Flow cytometry was used to detect the effect of shIDO1 + RT for 48 h on the apoptosis of lung adenocarcinoma cells. (H) Western blotting was used to detect the expression levels of apoptosis-related proteins. Data are presented as the mean ± SD. *P<0.05, **P<0.01, ***P<0.001 and ****P<0.0001 vs. Scr; $^{\#}$P<0.05 and $^{\#\#}$P<0.01. C-PARP, cleaved-poly [ADP-ribose] polymerase 1; D0, Day 0; IDO1, indoleamine-2,3-dioxygenase 1; KYN, kynurenine; ns, not significant; NSCLC, non-small cell lung cancer; RT, radiotherapy; Scr, scrambled shRNA negative control; sh/shRNA, short hairpin RNA.

at 48 h. IDO1 was mainly expressed in the nucleus, with a low expression in the cytoplasm. These findings indicated that IDO1 was upregulated in human lung cancer cells after exposure to radiation.

To determine the effects of IDO1 on the sensitivity of lung cancer cells to radiation, A549 and H1975 cells were collected and their radiosensitivity was investigated after IDO1 knockdown (Fig. 1D and E). Compared with the Scr cells, the

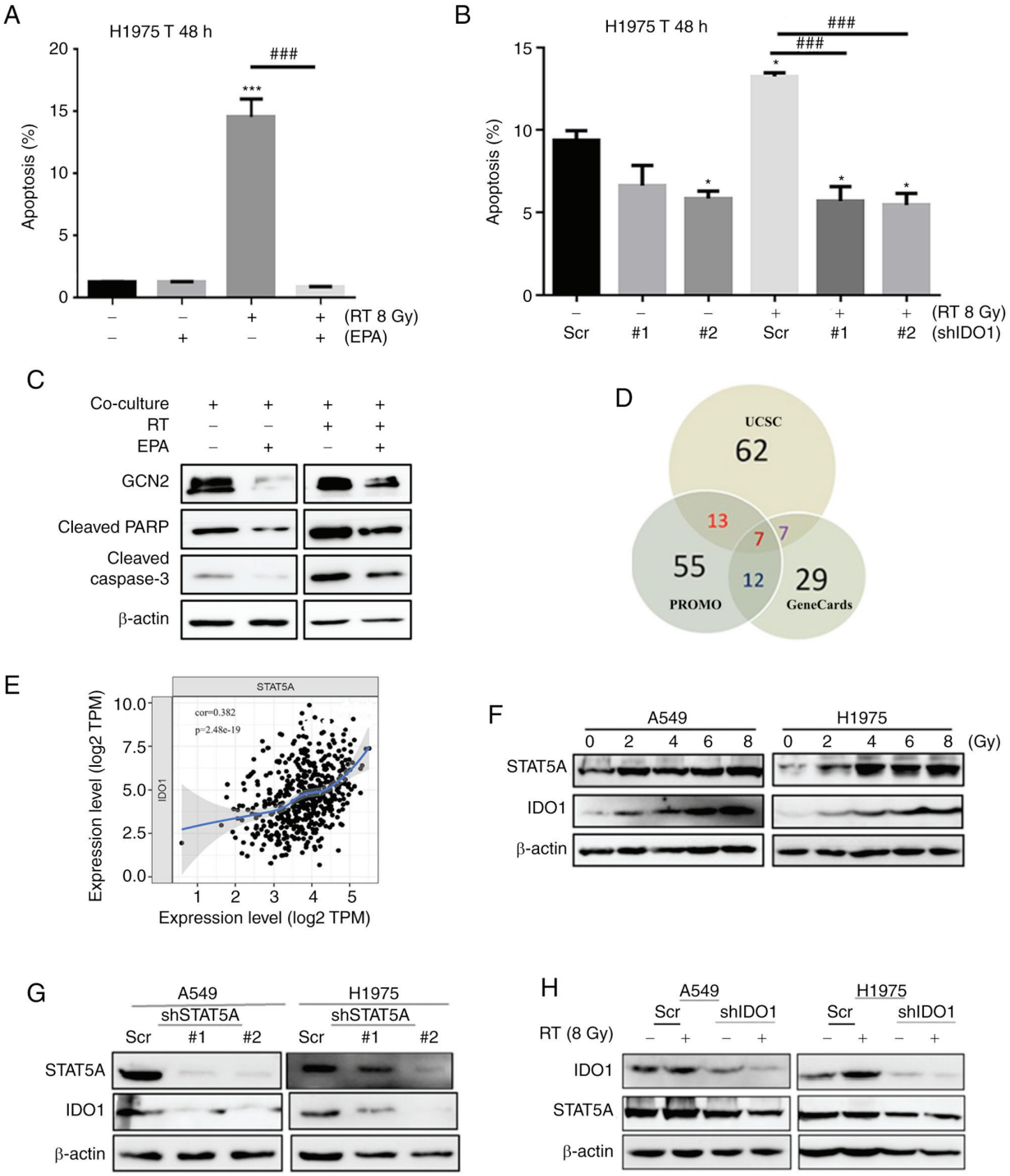

Figure 2. IDO1 inhibition reverses irradiation-induced apoptosis of Jurkat T cells, and STAT5A serves an important role in regulating the expression of IDO1. (A) H1975 cells were co-cultured with Jurkat T cells (1:4) and then exposed to 8 Gy radiation. Subsequently, the apoptotic rate of extracted Jurkat T cells was detected by flow cytometry. (B) Flow cytometry was used to detect the effect of shIDO1 combined with RT for 48 h on the apoptosis of Jurkat T cells. (C) Western blotting was used to detect the expression levels of apoptosis-related proteins and GCN2 downstream of IDO1. (D) Several databases (UCSC, PROMO and GeneCards) were used to predict the transcription factors that may regulate IDO1. (E) Positive correlation between the expression of STAT5A and IDO1 in patients with lung cancer in TIMER database. (F) Western blot analysis showed the effects of RT on the STAT5A expression in A549 and H1975 cells. (G) Western blot analysis showed that interfering with the expression of STAT5A decreased the expression levels of IDO1. (H) Western blot analysis showed that knocking down the expression of IDO1 did not affect STAT5A protein expression after irradiation. Data are presented as the mean ± SD. *P<0.05, ***P<0.001 vs. Scr; $^{###}$P<0.01. EPA, epacadostat; IDO1, indoleamine-2,3-dioxygenase 1; RT, radiotherapy; Scr, scrambled shRNA negative control; sh, short hairpin RNA.

number of IDO1 knockdown A549 and H1975 cell colonies was notably reduced as radiation dose increased (Fig. 1F). The sensitivity enhancement ratios for an estimated SF of IDO1 knockdown cells were 1.366 or 1.835 for shIDO1#1 and shIDO1#2 transduced A549 cells, respectively, and 1.166 or 1.286 for the two H1975 cell transductions. These results indicated that IDO1 knockdown sensitized lung cancer cells to radiation treatment.

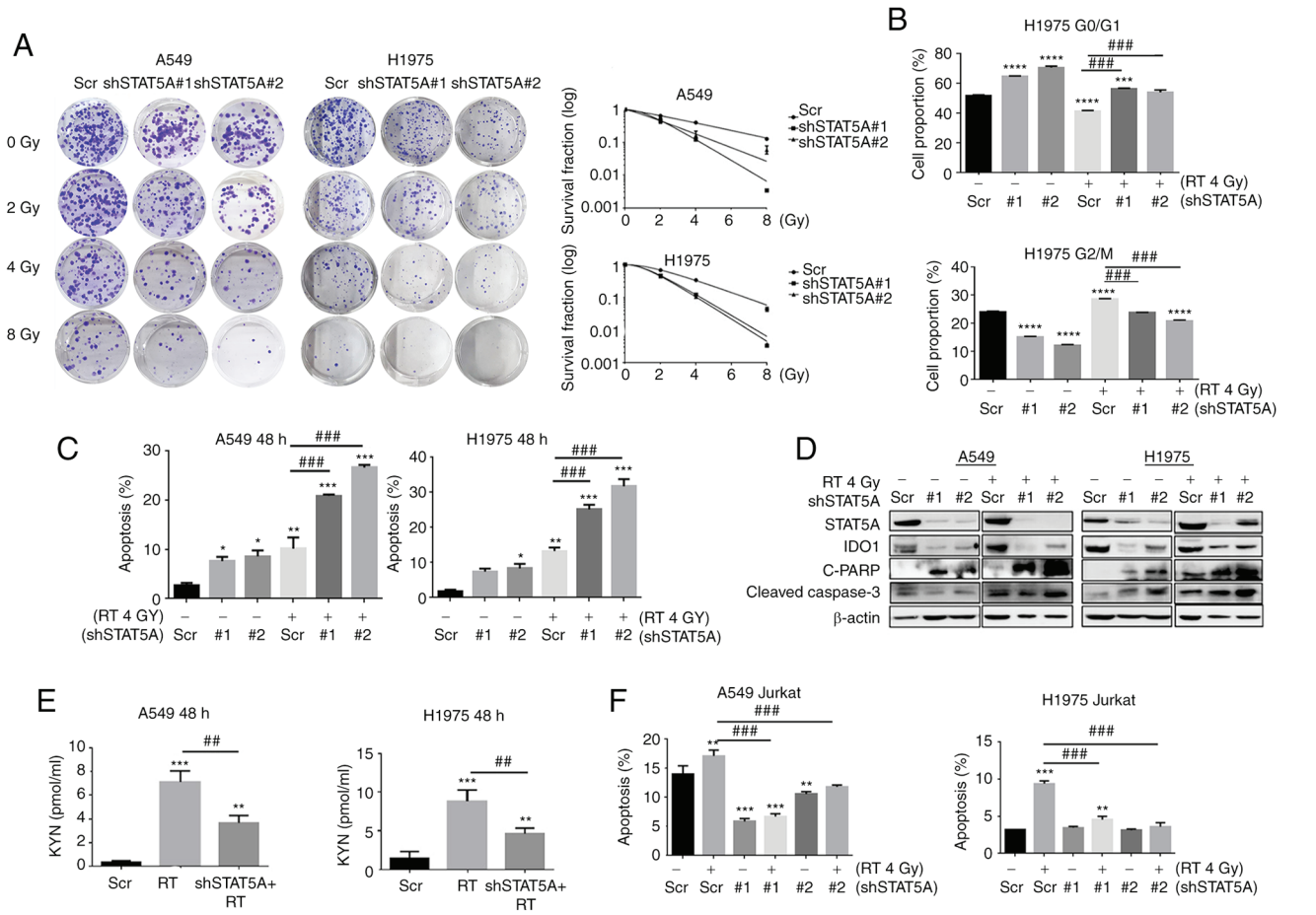

Figure 3. Effects of STAT5A knockdown in combination with RT on proliferation, cell cycle progression and apoptosis of lung cancer cells. (A) Cell survival was assessed via clonogenic assay to examine the radiosensitivity of transduced cells following irradiation (0, 2, 4 and 8 Gy). The diameter of each well is 35 mm. (B) Cell cycle arrest at the G_0/G_1 phase after shSTAT5A transduction. (C) Apoptosis was assessed by flow cytometry. (D) Western blotting was used to detect the expression levels of apoptosis-related proteins. (E) KYN was analyzed in the culture medium from A549 and H1975 transduced with shSTAT5A with or without RT exposure; the concentration of KYN was determined by ELISA. (F) Flow cytometry was used to detect the effect of shSTAT5A + RT for 48 h on the apoptosis of Jurkat cells. Data are presented as the mean ± SD. *P<0.05, **P<0.01, ***P<0.001 and ****P<0.0001 vs. Scr; $^{\#\#}$P<0.01 and $^{\#\#\#}$P<0.001. C-PARP, cleaved-poly [ADP-ribose] polymerase 1; CON, negative control; IDO1, indoleamine-2,3-dioxygenase 1; KYN, kynurenine; ns, not significant; RT, radiotherapy; Scr, scrambled shRNA negative control; sh, short hairpin RNA.

Flow cytometry was used to determine the efficacy of shIDO1 transduction combined with RT on the apoptotic rate of lung adenocarcinoma cells. The use of the combination was found to increase the radiation-induced lung adenocarcinoma cell apoptotic rate (Figs. 1G and S2). Western blot analysis showed that compared with the Scr group, the expression levels of apoptosis-related proteins [cleaved-caspase-3 and cleaved-Poly (ADP-ribose) polymerase 1 (PARP)] were significantly increased in RT + shIDO1 group (Fig. 1H).

Flow cytometry was also used to detect the apoptotic state of T cells in a co-culture system. H1975 cells were co-cultured with Jurkat T cells for 48 h after RT; the apoptotic rate was significantly higher compared with that in the non-RT group (Fig. 2A). When shIDO1 or EPA were used to suppress IDO1 in H1975 cells, the apoptotic rate of T cells in the RT combined with shIDO1 or EPA group was significantly lower compared with that in the RT alone group (Figs. 2A, B, S3A and B). Furthermore, under RT, when IDO1 expression was blocked with EPA, the expression levels of GCN2, cleaved-caspase-3 and cleaved-PARP were notably lower compared with the RT-only group, suggesting that RT-induced T-cell apoptosis may be IDO1-dependent (Fig. 2C).

STAT5A knockdown contributes to decreased IDO1 expression in NSCLC, and STAT5A knockdown enhances the survival of Jurkat T cells by suppressing IDO1 function. Databases (including UCSC, PROMO and GeneCards) were used to predict the transcription factors that may regulate IDO1 expression (Fig. 2D); seven transcription factors were identified that may bind to the promoter region of IDO1, including CEBPB, YY1, GATA1, SP1, STAT5A, STAT1 and STAT3. The expression of transcription factor STAT5A is significantly correlated with IDO1 in patients with lung cancer in the TIMER database (Fig. 2E). Western blot analysis demonstrated that the expression levels of STAT5A and IDO1 in lung adenocarcinoma cells following irradiation were comparable; that is, both expression levels were increased with higher radiation exposure (Fig. 2F). Interfering with STAT5A expression notably inhibited IDO1 expression (Fig. 2G); however, after IDO1 knockdown, STAT5A expression was not altered in tumor cell lines after irradiation (Fig. 2H). These

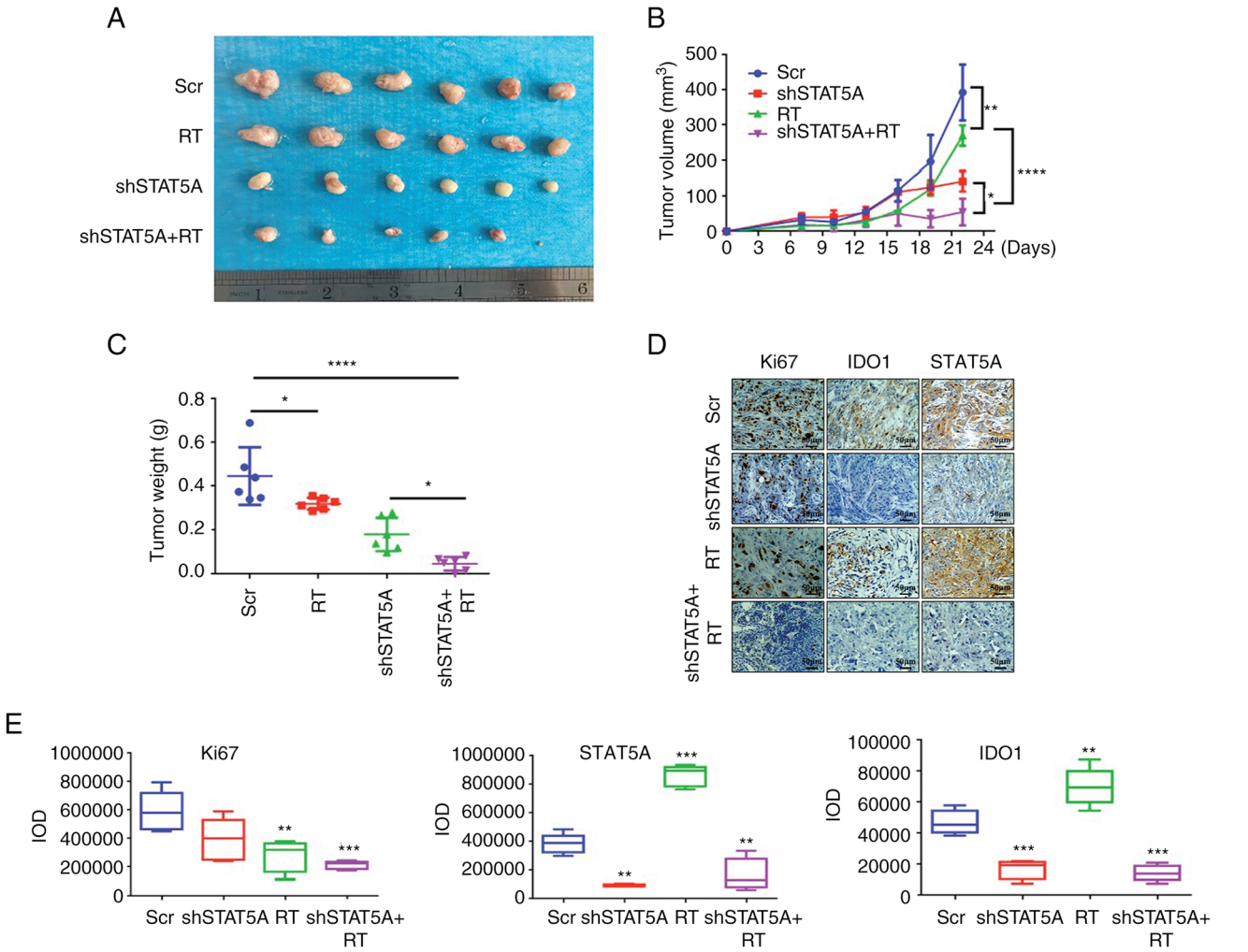

Figure 4. Effects of shSTAT5A combined with RT on BALB/c nude mice tumor formation and proliferation *in vivo*. (A) Images of excised subcutaneous xenografts from BALB/c nude mice injected with shSTAT5A-transduced H1975 cells. (B) Tumor volume was measured in all mice every 3 days. (C) Tumor weight was measured in all mice following excision. (D) Immunohistochemistry of Ki-67, IDO1 and STAT5A and were performed on the tumor samples (magnification, x200). (E) Semi-quantification of Ki67, STAT5A and IDO1 staining intensity in the images shown in (D). The experiments were repeated three times. Data are presented as the mean ± SD. *P<0.05, **P<0.01, ***P<0.001, ****P<0.0001 vs. Scr. IDO1, indoleamine-2,3-dioxygenase 1; IOD, integrated optical density; RT, radiotherapy; Scr, scrambled shRNA negative control; sh, short harpin RNA.

findings indicated that STAT5A may be a transcription factor that regulates IDO1 expression.

The function of STAT5A in RT of NSCLC *in vitro* was also explored. Results from the colony formation assay revealed that knockdown of STAT5A resulted in decreased proliferation and increased sensitivity to radiation therapy compared with the Scr group (Fig. 3A). As determined by flow cytometry, STAT5A knockdown resulted in cell cycle arrest at G_0/G_1 phase, whereas the number of cells at G0/G1 was significantly decreased in cells treated with RT alone compared with Scr group. Compared with RT alone, shSTAT5A + RT also resulted in cell cycle arrest at G_0/G_1 phase. The percentage of cells in the G2/M phase in the shSTAT5A groups were significantly decreased, whereas RT alone resulted in cell cycle arrest at G2/M phase compared with the Scr group. Compared with RT alone, shSTAT5A + RT also decreased the percentage of cells in the G2/M phase (Figs. 3B and S4). Flow cytometric apoptosis analysis showed that shSTAT5A combined with RT significantly increased the total apoptotic rate of the two cell lines compared with RT alone (Figs. 3C and S5). Western blot analysis also revealed that the expression levels of apoptosis-related proteins (cleaved-caspase-3 and cleaved-PARP) in shSTAT5A + RT were markedly increased compared with RT alone (Fig. 3D).

The influence and potential underlying molecular mechanism of shSTAT5A + RT on IDO1 enzyme activity and T-lymphocyte apoptotic rate in the co-culture system was further investigated using ELISA and flow cytometry. The ELISA results of the culture medium of A549 and H1975 cells showed that RT enhanced KYN compared with the Scr group, whereas shSTAT5A + RT suppressed KYN compared with RT alone (Fig. 3E). Furthermore, flow cytometry suggested that the group treated with Scr + RT exhibited an enhanced percentage of apoptotic Jurkat T cells compared with the Scr group (Figs. 3F and S6). Moreover, the shSTAT5A + RT group demonstrated a reverse in the apoptosis of Jurkat T cells compared with the Scr + RT group. Taken together, these results indicated that shSTAT5A may suppress the apoptosis of Jurkat T cells by blocking IDO1 expression.

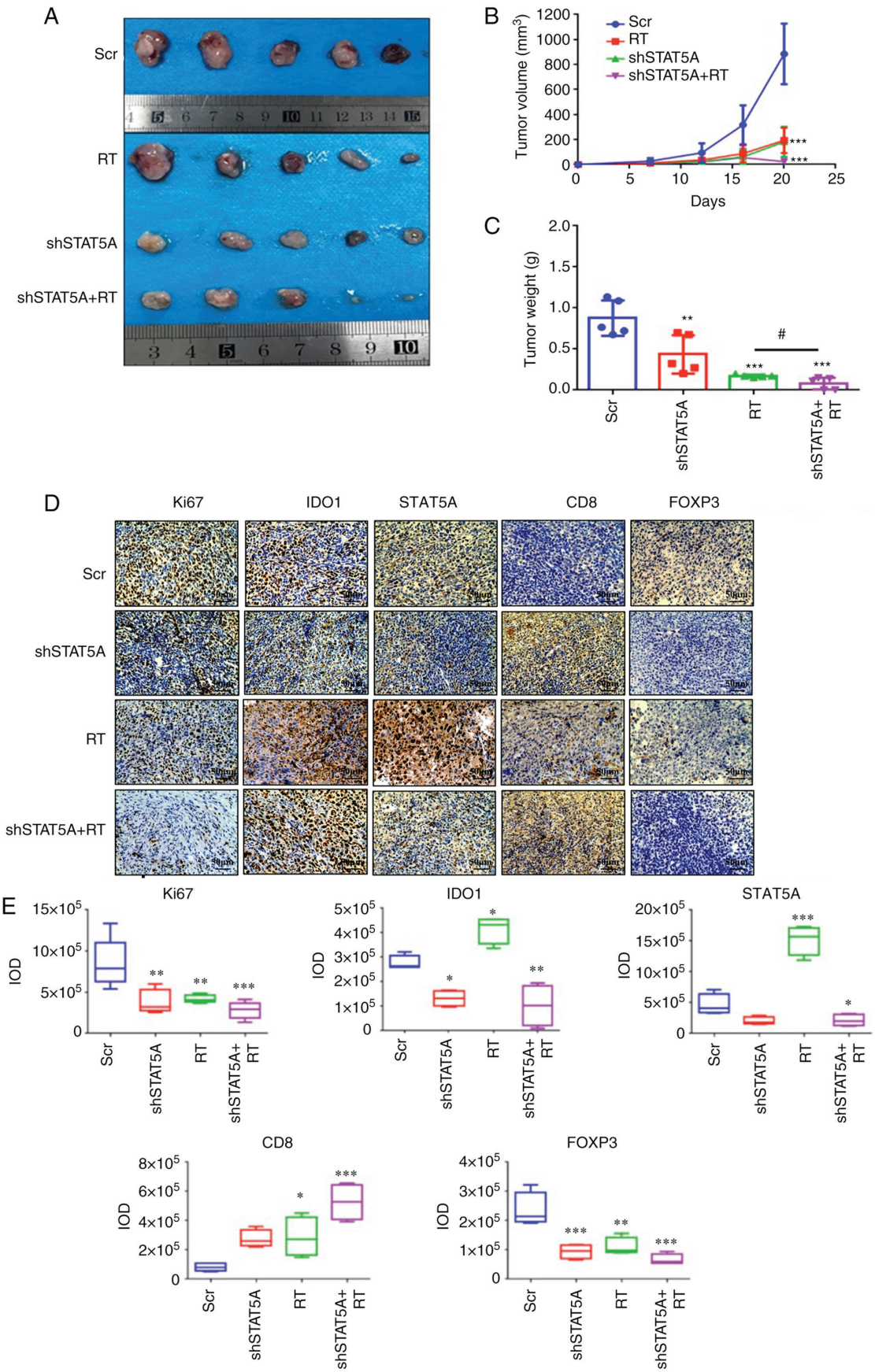

Figure 5. Effects of shSTAT5A combined with RT on C57BL/6 mice xenograft tumor formation and proliferation *in vivo*. (A) Images of excised subcutaneous xenografts of C57BL/6 mice injected with shSTAT5A-transduced LLC cells. (B) Tumor volume was measured in all mice twice a week. (C) Tumor weight was measured in all mice. (D) Immunohistochemistry of Ki-67, IDO1, STAT5A, CD8 and FOXP3 were performed on the tumor samples (magnification, x200). (E) Semi-quantification of Ki67, IDO1, STAT5A, CD8 and FOXP3, staining intensity in the images shown in (D). The experiments were repeated three times. Data are presented as the mean ± SD. *P<0.05, **P<0.01, ***P<0.001 vs. Scr, $^{\#}$P<0.05. FOXP3; forkhead box P3; IDO1, indoleamine-2,3-dioxygenase 1; IOD, integrated optical density; LLC, Lewis lung carcinoma; RT, radiotherapy; Scr, scrambled shRNA negative control; sh, short harpin RNA.

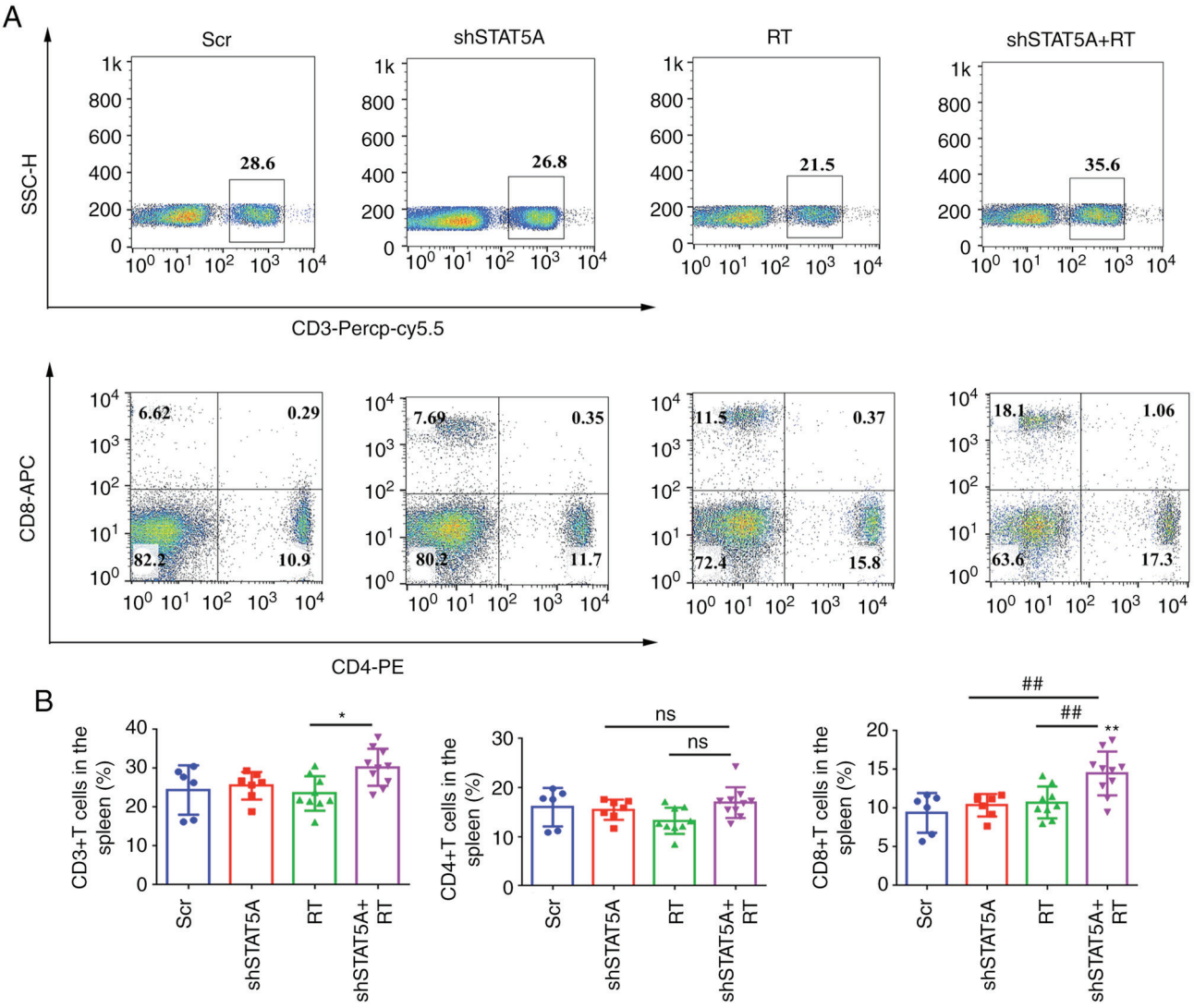

Figure 6. Knockdown of STAT5A combined with RT promoted the activation of CD8$^+$T cell response in spleen. (A) Representative flow cytometry plots of CD3$^+$, CD4$^+$ and CD8$^+$ T cells and (B) quantitative analysis of the results of CD3$^+$, CD4$^+$ and CD8$^+$ T cells in the spleen. Data are presented as the mean ± SD. *P<0.05, **P<0.01 vs. Scr; $^{\#\#}$P<0.01. APC, allophycocyanin; Cy, cyanine; ns, not significant; PE, phycoerythrin; PerCP, peridinin chlorophyll protein; RT, radiotherapy; Scr, scrambled shRNA negative control; sh, short hairpin RNA; SSC, side scatter.

Knockdown of STAT5A combined with RT significantly inhibits the growth of NSCLC tumors in vivo. NCI-H1975 and LLC cells were transduced with shSTAT5A and were then injected subcutaneously into immune-compromised mice (BALB/c nude) and mice with a functioning immune system (C57BL/6). Results showed that shSTAT5A#1 and shSTAT5A#2 notably decreased the protein levels of STAT5A in LLC cell (Fig. S7A). Mice were divided into the following four groups: Scr, RT, shSTAT5A and shSTAT5A + RT; the mice were sacrificed and tumors were harvested (Figs. 4A and 5A). For BALB/c nude mice, compared with Scr group, tumor growth was significantly inhibited in the other three groups. Additionally, compared with RT group, the shSTAT5A + RT group exhibited more impeded tumor growth (Fig. 4B). For C57BL/6 mice, compared with Scr group, the other three groups significantly inhibited the tumor growth; however, there was no difference between the treatment groups (Fig. 5B). In addition, the average tumor weight in the shSTAT5A + RT groups were significantly lower compared with those in the Scr group (Figs. 4C and 5C). Notably, there were no detectable effects of each treatment regimen on body weights of the treated mice (Fig. S7B).

IHC staining in the sections of LLC tumors revealed that shSTAT5A + RT significantly inhibited STAT5A and Ki67 protein levels in BALB/c nude (Fig. 4D and E) and C57BL/6 models compared with the Scr group (Fig. 5D and E). IHC staining also demonstrated that the combined shSTAT5A + RT treatment resulted in a reduction in IDO1 expression, an increase in the number of CD8$^+$ T cells and a decrease in the number FOXP3$^+$ Tregs compared with the Scr treatment (Fig. 5D and E). These data indicated that shSTAT5A + RT may significantly attenuate tumor growth *in vivo*, probably through a mechanism involving an increased recruitment or activation of cytotoxic T cells and a reduced recruitment or activation of inhibitory Tregs.

Knockdown of STAT5A combined with RT promotes activation of the antitumor T-cell response in vivo. The

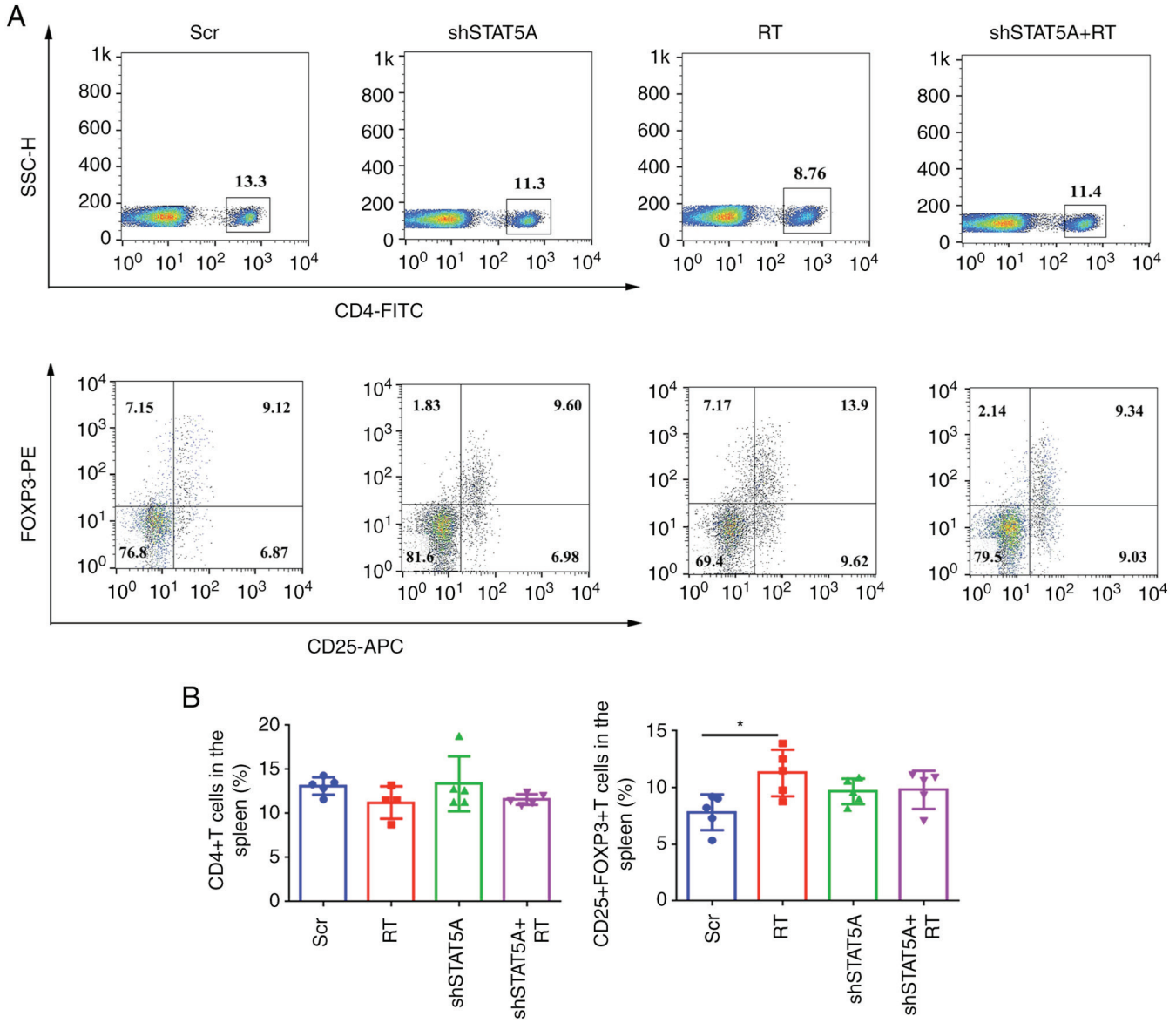

Figure 7. Knockdown of STAT5A combined with RT did not decrease Tregs in the spleen. (A) Representative flow cytometry plots and (B) quantitative analysis results of $CD25^+FOXP3^+CD4^+$ Tregs in the spleen. Data are presented as the mean ± SD. $^*P<0.05$. FOXP3, forkhead box P3; ns, not significant; RT, radiotherapy; Scr, scrambled shRNA negative control; sh, short hairpin RNA; Tregs, regulatory T cells.

abundance of total $CD3^+$, $CD4^+$ and $CD8^+$ T-cell subsets in the spleen and dissociated LLC tumor tissue from C57BL/6 mice was assessed using flow cytometry. Compared with RT-treated mice, shSTAT5A + RT resulted in a significant increase in the percentage of $CD3^+$ T cells in the spleen (Fig. 6A and B); there was no significant difference in $CD4^+$ T cells among the four treatment groups, whereas the number of $CD8^+$ T cells was significantly higher in the shSTAT5A + RT group compared with in the other three groups. In the tumors, shSTAT5A + RT had no significant effect on $CD3^+$ T cells, and there was no significant difference among the four treatment groups (Fig. S8A and B). Notably, the number of $CD4^+$ T cells was decreased in the shSTAT5A + RT group compared with the Scr group, whereas the number of $CD8^+$ T cells was increased (Fig. S8A and B).

To determine other potential mechanisms underlying the induction of immunosuppression, the present study analyzed the changes in the abundance of Tregs in mouse spleen and tumor tissues using flow cytometry. The results revealed that, compared with the Scr group, the number of $CD25^+FOXP3^+CD4^+$ Tregs in the spleens of mice in the RT group were significantly increased, whereas no significant difference was identified in the shSTAT5A and shSTAT5A + RT groups compared with Scr (Fig. 7A and B). Compared with the Scr group, $CD25^+FOXP3^+CD4^+$ Treg infiltration in mouse tumors was significantly reduced in the shSTAT5A + RT group (Fig. S9A and B). Collectively, these data suggested that knockdown of STAT5A combined with RT may promote activation of the antitumor T-cell response *in vivo*.

Discussion

RT serves an important role in the treatment of NSCLC (10,36). In addition to RT and chemotherapy, immunotherapy has attracted much attention. Immune checkpoint inhibitors have shown significant clinical efficacy in the treatment of NSCLC;

nevertheless, drug resistance may occur, and the long-term survival of patients with NSCLC remains unsatisfactory (37). Therefore, an in-depth understanding of the molecular mechanism underlying RT resistance is vital, and potential reversal strategies urgently need to be resolved for current lung cancer treatment.

A previous study has reported that IDO1 contributes to tumor progression *in vivo* by suppressing tumor-infiltrating T lymphocytes and natural killer cells, and by activating Tregs (38). In addition to suppressing the antitumor immune response, IDO1 may promote tumor development in a non-immunomodulating manner. The inhibition of IDO1 expression has been shown to sensitize human lung cancer cells to chemotherapeutic agents by regulating the cell cycle (39). In colorectal cancer cells, it was found that TRP metabolites activate the β-catenin pathway and promote cell proliferation (40). The present study revealed that IDO1 expression was increased after RT, and interfering with the expression of IDO1 reduced proliferation, promoted apoptosis and promoted the inherent antitumor effect of radiation on lung cancer cells. These results were similar to those of a prior study wherein IDO1 inhibition was found to sensitize colorectal cancer cells to radiation-induced cell death (41). When the activity or concentration of local IDO1 increases, TRP in the cell is metabolized to KYN, resulting in a significant reduction in TRP concentration (24). In the state of low TRP levels, tryptophanyl tRNA concentration increases, which activates GCN2 (26). In the present study, tumor cells and Jurkat T cells were co-cultured, and it was revealed that RT could upregulate IDO1 of lung cells, increase the content of KYN, and ultimately induce T-cell apoptosis. IDO1 knockdown or the use of IDO1 inhibitors was able to hinder T-cell apoptosis. These data indicated that an RT-induced increase in IDO1 expression in lung cells may be a factor leading to T-cell apoptosis.

A previous report showed that an IL-6-induced proto-oncogene protein, intestinal-specific homeobox, can induce the expression of IDO1 and TDO, thereby increasing KYN and aryl hydrocarbon receptor levels, and promoting the expression of CD86 and PD-L1 in liver cancer cells (42). The present study predicted that STAT5A is an upstream transcription factor affecting IDO1 expression. Moreover, it was confirmed that RT significantly promoted the expression levels of STAT5A and IDO1. Interfering with IDO1 did not affect the expression of STAT5A, whereas interfering with STAT5A prevented a radiation-induced increase in IDO1 expression, thereby significantly improving the radiosensitivity of lung cancer cells.

To further evaluate the effects of the STAT5A/IDO1 axis on the efficacy of RT in lung cancer treatment, two cell-line derived xenograft mouse models (BALB/c nude and C57BL/6) were selected for *in vivo* analysis in the present study. The results demonstrated that shSTAT5A combined with RT decreased tumor volume and weight, as well as significantly suppressed tumor cell proliferation in these mouse models, as determined by Ki67 IHC. Moreover, in the C57BL/6 model, STAT5A knockdown sensitized tumors to RT by decreasing IDO1 expression, reducing FOXP3 and recruiting infiltrating $CD8^+$ T cells that drive the antitumor immune response. In the occurrence and development of tumors, $CD25^+FOXP3^+CD4^+$ Tregs can hinder the effect of antitumor immunity by inducing $CD8^+$ T cell dysfunction and depletion (37). Tregs in the TME have a stronger inhibitory effect than Tregs in the spleen and peripheral blood (43). It has previously been reported that 2 Gy RT can increase the proportion of Tregs in the spleen. Increasing the RT dose to 20 Gy can double the proportion of Tregs infiltrating the tumors (44). However, some studies have reported that Tregs show dose-dependent apoptosis with an increase in irradiation dose, which downregulates the expression levels of FOXP3, CD25 and CTLA-4, and which may weaken their ability to inhibit the proliferation of $CD8^+$ T cells (45,46). The present study demonstrated that the C57BL/6 mouse model of lung cancer had some of the same characteristics as other solid tumors, such as rich Treg infiltration. STAT5A knockdown with 8 Gy RT reduced the infiltration of $CD25^+FOXP3^+CD4^+$ Tregs, thereby enhancing the proportion of $CD8^+$ T cells. Targeting the expression of STAT5A/IDO1 may effectively prevent Treg infiltration and provide a novel idea for inhibiting the RT-induced immunosuppressive microenvironment.

In conclusion, the present study demonstrated that IDO1 and STAT5A were highly expressed in cancer tissues. The expression levels of both proteins were positively related to the immune microenvironment. RT significantly promoted the expression levels of STAT5A and IDO1 in NSCLC, and their activity supported the apoptosis of T cells. In addition, the results confirmed that STAT5A knockdown may promote activation of the antitumor T-cell response by regulating IDO1 expression. In this context, a regulatory mechanism of STAT5A/IDO1 in RT-mediated immunosuppression was proposed, which may provide insight into the development of more comprehensive immunotherapy regimens for patients with NSCLC.

Acknowledgements

Not applicable.

Funding

This work was supported by The National Natural Science Foundation of China (grant no. 81372436), The Scientific and Technological Project in Henan Province (grant no. 222102310015), and The Medical Science and Technology Project in Henan Province (grant no. SBGJ202102056).

Availability of data and materials

The datasets used and/or analyzed during the current study are available from the corresponding author on reasonable request.

Authors' contributions

HG and ZD designed the experiments. YY, XZ, PN, DL and QD collected the specimens and performed the experiments. YY, XW, YW, YS, and KL analyzed the statistical data. All authors read and approved the final manuscript.

Ethics approval and consent to participate

The present study was approved by the Animal Care and Use Committee of Zhengzhou University (Zhengzhou, China; NO.CUHCI2021-003).

Patient consent for publication

Not applicable.

Competing interests

The authors declare that they have no competing interests.

References

1. Siegel RL, Miller KD, Fuchs HE and Jemal A: Cancer statistics, 2021. CA Cancer J Clin 71: 7-33, 2021.
2. Global Burden of Disease Cancer Collaboration, Fitzmaurice C, Akinyemiju TF, Al Lami FH, Alam T, Alizadeh-Navaei R, Allen C, Alsharif U, Alvis-Guzman N, Amini E, *et al*: Global, regional, and national cancer incidence, mortality, years of life lost, years lived with disability, and disability-adjusted life-years for 29 cancer groups, 1990 to 2016: A systematic analysis for the global burden of disease study. JAMA Oncol 4: 1553-688, 2018.
3. Chen Y, Peng X, Zhou Y, Xia K and Zhuang W: Comparing the benefits of chemoradiotherapy and chemotherapy for resectable stage III A/N2 non-small cell lung cancer: A meta-analysis. World J Surg Oncol 16: 8, 2018.
4. Herbst RS, Morgensztern D and Boshoff C: The biology and management of non-small cell lung cancer. Nature 553: 446-454, 2018.
5. Reck M and Rabe KF: Precision diagnosis and treatment for advanced non-small-cell lung cancer. N Engl J Med 377: 849-861, 2017.
6. Herrera FG, Bourhis J and Coukos G: Radiotherapy combination opportunities leveraging immunity for the next oncology practice. CA Cancer J Clin 67: 65-85, 2017.
7. Chen Y, Gao M, Huang Z, Yu J and Meng X: SBRT combined with PD-1/PD-L1 inhibitors in NSCLC treatment: A focus on the mechanisms, advances, and future challenges. J Hematol Oncol 13: 105, 2020.
8. Ngwa W, Irabor OC, Schoenfeld JD, Hesser J, Demaria S and Formenti SC: Using immunotherapy to boost the abscopal effect. Nat Rev Cancer 18: 313-322, 2018.
9. Horn L, Mansfield AS, Szczęsna A, Havel L, Krzakowski M, Hochmair MJ, Huemer F, Losonczy G, Johnson ML, Nishio M, *et al*: First-line atezolizumab plus chemotherapy in extensive-stage small-cell lung cancer. N Engl J Med 379: 2220-2229, 2018.
10. Brooks ED and Chang JY: Time to abandon single-site irradiation for inducing abscopal effects. Nat Rev Clin Oncol 16: 123-135, 2019.
11. Zheng X, Sun Y, Ye K, Fan C, Wang X, Yang Y, Jiao R and Ge H: Stereotactic ablative radiotherapy as single treatment for early stage non-small cell lung cancer: A single institution analysis. Thoracic Cancer 12: 899-905, 2021.
12. Zheng XL, Liu ML, Wang XH, Sun Y, Song S, Yang Y, Jiao R, Ye K, Fan C and Ge H : Analysis of clinical outcomes and prognostic factors in 109 patients with early-stage non-small cell lung cancer treated with stereotactic ablation radiotherapy. Chin J Radiat Oncol 29: 1031-1036, 2020 (In Chinese).
13. Gettinger SN, Horn L, Gandhi L, Spigel DR, Antonia SJ, Rizvi NA, Powderly JD, Heist RS, Carvajal RD, Jackman DM, *et al*: Overall survival and long-term safety of nivolumab (anti-programmed death 1 antibody, BMS-936558, ONO-4538) in patients with previously treated advanced non-small-cell lung cancer. J Clin Oncol 33: 2004-2012, 2015.
14. Procureur A, Simonaggio A, Bibault JE, Oudard S and Vano YA: Enhance the immune checkpoint inhibitors efficacy with radiotherapy induced immunogenic cell death: A comprehensive review and latest developments. Cancers (Basel) 13: 678, 2021.
15. Theelen WSME, Chen D, Verma V, Hobbs BP, Peulen HMU, Aerts JGJV, Bahce I, Niemeijer ALN, Chang JY, de Groot PM, *et al*: Pembrolizumab with or without radiotherapy for metastatic non-small-cell lung cancer: A pooled analysis of two randomised trials. Lancet Respir Med 9: 467-475, 2021.
16. Zhou QH, Han H, Lu JB, Liu TY, Huang KB, Deng CZ, Li ZS, Chen JP, Yao K, Qin ZK, *et al*: Up-regulation of indoleamine 2,3-dioxygenase 1 (IDO1) expression and catalytic activity is associated with immunosuppression and poor prognosis in penile squamous cell carcinoma patients. Cancer Commun (Lond) 40: 3-15, 2020.
17. Wei L, Wu N, Wei F, Li F, Zhang Y, Liu J and Ren X: Prognosis significance of indoleamine 2, 3-dioxygenase, programmed death ligand-1 and tumor-infiltrating immune cells in microenvironment of breast cancer. Int Immunopharmacol 84: 106506, 2020.
18. Brandacher G, Perathoner A, Ladurner R, Schneeberger S, Obrist P, Winkler C, Werner ER, Werner-Felmayer G, Weiss HG, Göbel G, *et al*: Prognostic value of indoleamine 2,3-dioxygenase expression in colorectal cancer: Effect on tumor-infiltrating T cells. Clin Cancer Res 12: 1144-1151, 2006.
19. Kiyozumi Y, Baba Y, Okadome K, Yagi T, Ishimoto T, Iwatsuki M, Miyamoto Y, Yoshida N, Watanabe M, Komohara Y and Baba H: IDO1 expression is associated with immune tolerance and poor prognosis in patients with surgically resected esophageal cancer. Ann Surg 269: 1101-1108, 2019.
20. Halaby MJ, Hezaveh K, Lamorte S, Ciudad MT, Kloetgen A, MacLeod BL, Guo M, Chakravarthy A, Medina TDS, Ugel S, *et al*: GCN2 drives macrophage and MDSC function and immunosuppression in the tumor microenvironment. Sci Immunol 4: eaax8189, 2019.
21. Zhu YY, Hu M, Xu QH, Sun X, Ye Y, Liu Y, Feng J and Xu Y: The correlation between serum indoleamine 2,3-dioxygenase and the prognosis of stereotactic radiotherapy for early non-small cell lung cancer. Chin J Radiol Med Prot 40: 512-518, 2020 (In Chinese).
22. Jiao R, Zheng X, Sun Y, Feng Z, Song S and Ge H: IDO1 expression increased after neoadjuvant therapy predicts poor pathologic response and prognosis in esophageal squamous cell carcinoma. Front Oncol 10: 1099, 2020.
23. Le Naour J, Galluzzi L, Zitvogel L, Kroemer G and Vacchelli E: Trial watch: IDO inhibitors in cancer therapy. Oncoimmunology 9: 1777625, 2020.
24. Li A, Barsoumian HB, Schoenhals JE, Caetano MS, Wang X, Menon H, Valdecanas DR, Niknam S, Younes AI, Cortez MA and Welsh JW: IDO1 inhibition overcomes radiation-induced 'rebound immune suppression' by reducing numbers of IDO1-expressing myeloid-derived suppressor cells in the tumor microenvironment. Int J Radiat Oncol Biol Phys 104: 903-912, 2019.
25. Grobben Y, de Man J, van Doornmalen AM, Muller M, Willemsen-Seegers N, Vu-Pham D, Mulder WR, Prinsen MBW, de Wit J, Sterrenburg JG, *et al*: Targeting indoleamine 2,3-dioxygenase in cancer models using the novel small molecule inhibitor NTRC 3883-0. Front Immunol 11: 609490, 2021.
26. Kocher F, Amann A, Zimmer K, Geisler S, Fuchs D, Pichler R, Wolf D, Kurz K, Seeber A and Pircher A: High indoleamine-2,3-dioxygenase 1 (IDO) activity is linked to primary resistance to immunotherapy in non-small cell lung cancer (NSCLC). Transl Lung Cancer Res 10: 304-313, 2021.
27. Maurer B, Kollmann S, Pickem J, Hoelbl-Kovacic A and Sexl V: STAT5A and STAT5B-twins with different personalities in hematopoiesis and leukemia. Cancers (Basel) 11: 1726, 20019.
28. Koptyra M, Gupta S, Talati P and Nevalainen MT: Signal transducer and activator of transcription 5a/b: Biomarker and therapeutic target in prostate and breast cancer. Int J Biochem Cell Biol 43: 1417-1421, 2011.
29. Brachet-Botineau M, Deynoux M, Vallet N, Polomski M, Juen L, Hérault O, Mazurier F, Viaud-Massuard MC, Prié G and Gouilleux F: A novel inhibitor of STAT5 signaling overcomes chemotherapy resistance in myeloid leukemia cells. Cancers (Basel) 11: 2043, 2019.
30. Sánchez-Ceja SG, Reyes-Maldonado E, Vázquez-Manríquez ME, López-Luna JJ, Belmont A and Gutiérrez-Castellanos S: Differential expression of STAT5 and Bcl-xL, and high expression of Neu and STAT3 in non-small-cell lung carcinoma. Lung Cancer 54: 163-168, 2006.
31. Maranto C, Udhane V, Hoang DT, Gu L, Alexeev V, Malas K, Cardenas K, Brody JR, Rodeck U, Bergom C, *et al*: STAT5A/B blockade sensitizes prostate cancer to radiation through inhibition of RAD51 and DNA repair. Clin Cancer Res 24: 1917-1931, 2018.
32. Chang JY, Senan S, Paul MA, Mehran RJ, Louie AV, Balter P, Groen HJ, McRae SE, Widder J, Feng L, *et al*: Stereotactic ablative radiotherapy versus lobectomy for operable stage I non-small-cell lung cancer: A pooled analysis of two randomised trials. Lancet Oncol 16: 630-637, 2015.
33. Livak KJ and Schmittgen TD: Analysis of relative gene expression data using real-time quantitative PCR and the 2(-Delta C(T)) method. Methods 25: 402-408, 2001.

34. Low HY, Lee YC, Lee YJ, Wang HL, Chen YI, Chien PJ, Li ST and Chang WW: Reciprocal regulation between indoleamine 2,3-dioxigenase 1 and notch1 involved in radiation response of cervical cancer stem cells. Cancers (Basel) 12: 1547, 2020.
35. Lou Q, Liu R, Yang X, Li W, Huang L, Wei L, Tan H, Xiang N, Chan K, Chen J and Liu H: miR-448 targets IDO1 and regulates $CD8^+$ T cell response in human colon cancer. J Immunother Cancer 7: 210, 2019.
36. Palma DA, Olson R, Harrow S, Gaede S, Louie AV, Haasbeek C, Mulroy L, Lock M, Rodrigues GB, Yaremko BP, *et al*: Stereotactic ablative radiotherapy versus standard of care palliative treatment in patients with oligometastatic cancers (SABR-COMET): A randomised, phase 2, open-label trial. Lancet 393: 2051-2058, 2019.
37. Crittenden M, Kohrt H, Levy R, Jones J, Camphausen K, Dicker A, Demaria S and Formenti S: Current clinical trials testing combinations of immunotherapy and radiation. Semin Radiat Oncol 25: 54-64, 2015.
38. Maleki Vareki S, Rytelewski M, Figueredo R, Chen D, Ferguson PJ, Vincent M, Min W, Zheng X and Koropatnick J: Indoleamine 2,3-dioxygenase mediates immune-independent human tumor cell resistance to olaparib, gamma radiation, and cisplatin. Oncotarget 5: 2778-2791, 2014.
39. Thaker AI, Rao MS, Bishnupuri KS, Kerr TA, Foster L, Marinshaw JM, Newberry RD, Stenson WF and Ciorba MA: IDO1 metabolites activate β-catenin signaling to promote cancer cell proliferation and colon tumorigenesis in mice. Gastroenterology 145: 416-425.e1-e4, 2013.
40. Chen B, Alvarado DM, Iticovici M, Kau NS, Park H, Parikh PJ, Thotala D and Ciorba MA: Interferon-induced IDO1 mediates radiation resistance and is a therapeutic target in colorectal cancer. Cancer Immunol Res 8: 451-464, 2020.
41. Wang LT, Chiou SS, Chai CY, His E, Yokoyama KK, Wang SN, Huang SK and Hsu SH: Intestine-specific homeobox gene ISX integrates IL6 signaling, tryptophan catabolism, and immune suppression. Cancer Res 77: 4065-4077, 2017.
42. Maj T, Wang W, Crespo J, Zhang H, Wang W, Wei S, Zhao L, Vatan L, Shao I, Szeliga W, *et al*: Oxidative stress controls regulatory T cell apoptosis and suppressor activity and PD-L1-blockade resistance in tumor. Nat Immunol 18: 1332-1341, 2017.
43. Maruyama T, Li J, Vaque JP, Konkel JE, Wang W, Zhang B, Zhang P, Zamarron BF, Yu D, Wu Y, *et al*: Control of the differentiation of regulatory T cells and T(H)17 cells by the DNA-binding inhibitor Id3. Nat Immunol 12: 86-95, 2011.
44. Zhang T, Yu H, Ni C, Zhang T, Liu L, Lv Q, Zhang Z, Wang Z, Wu D, Wu P, *et al*: Hypofractionated stereotactic radiation therapy activates the peripheral immune response in operable stage I non-small-cell lung cancer. Sci Rep 7: 4866, 2017.
45. Cao M, Cabrera R, Xu Y, Liu C and Nelson D: Gamma irradiation alters the phenotype and function of CD4+CD25+ regulatory T cells. Cell Biol Int 33: 565-571, 2009.
46. Mortezaee K, Parwaie W, Motevaseli E, Mirtavoos-Mahyari H, Musa AE, Shabeeb D, Esmaely F, Najafi M and Farhood B: Targets for improving tumor response to radiotherapy. Int Immunopharmacol 76: 105847, 2019.